2013 IEEE/RSJ International Conference on
Intelligent Robots and Systems (IROS)
November 3-7, 2013. Tokyo, Japan

Carrying a Flexible Payload with Multiple Flying Vehicles

Robin Ritz and Raffaello D'Andrea

Abstract— **This paper introduces a method for carrying a flexible payload with multiple attached flying vehicles. A model for a particular class of flexible structures is presented, and an estimator is derived that observes the pose of the structure in space as well as the magnitude of some characteristic deformation modes. A control strategy that controls the flexible payload to a desired pose while also controlling the deformations to zero is introduced. The presented methods are validated in the ETH Zurich Flying Machine Arena by flying with a thin, flexible ring that is carried by six quadrocopters.**

I. Introduction

The need for aerial transport of a payload arises in many applications, and thanks to recent improvements in relevant technologies, autonomous aerial vehicles have become a plausible tool for achieving this task. However, due to the small size of most autonomous aerial vehicles, their payload capability is limited. To overcome this limitation, multiple agents can be used to cooperatively carry the same object. An example that has been studied extensively and applied successfully for various scenarios is cooperative aerial towing: transporting a payload connected to multiple flying vehicles via cables (see for example [1], [2], and references therein). Advantages of aerial towing are, for example, the easy way to attach and release the payload, and the relatively high distance between the payload and the vehicle such that the vehicle's aerodynamics are not considerably disturbed. On the other hand, connections via cables introduce additional dynamics that must be taken into account during controller design, and which may lower maneuverability. In order to avoid these additional dynamics, and to enable a more direct control of the payload, various approaches for carrying objects with rigidly attached vehicles have been developed and successfully demonstrated (examples include [3], [4], [5]). However, even if the vehicles are attached rigidly, the payload may be subject to some characteristic deformations and oscillations. A variety of methods for controlling flexible payloads with different characteristics has been introduced, see for example [6], [7]. In this paper, we introduce a method based on common techniques, for carrying such a flexible payload by using flying vehicles attached to it. The presented algorithm controls the object to a desired position and attitude, and at the same time suppresses some characteristic deformation modes. Fig. 1 shows the flexible structure that is used to demonstrate the validity of the methods presented herein: six quadrocopters attached to a flying ring.

This research was supported by the Hans-Eggenberger Stiftung and the SNSF (Swiss National Science Foundation). The authors are with the Institute for Dynamic Systems and Control, ETH Zürich.
{rritz, rdandrea}@ethz.ch

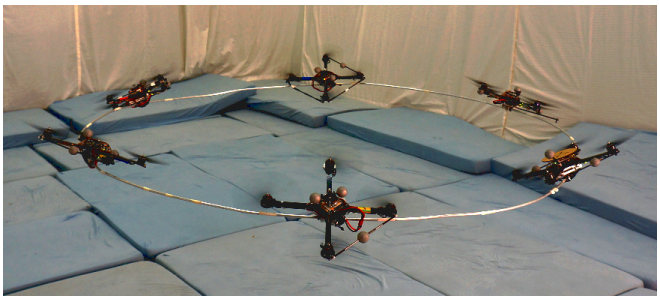

Fig. 1. Six quadrocopters carrying a thin, flexible ring. The ring is subject to characteristic bending modes that must be taken into account during controller design.

The remainder of this paper is structured as follows: The dynamical model for a particular class of flexible payloads is derived in Section II. Section III introduces an observer that provides full state information, including the current magnitude of the deformations. In Section IV, we present a control strategy for directing the flying, flexible structure to a desired pose[1], while also controlling the characteristic deformations to zero. In Section V we show experimental results of a flying ring, and we present conclusions in Section VI.

II. Model

This section derives the dynamical model for a particular class of flexible structures that are carried by a fleet of attached vehicles.

A. Attitude Representation

Throughout this paper we use the four-dimensional unit quaternion to represent attitudes. The reason for that is the well-known fact that all three-parameter attitude representations are singular or discontinuous [8]. In the dynamical model introduced below, the vehicles are attached to the payload with an arbitrary attitude, i.e. singular attitude representations should be avoided. Furthermore, even though the observer derived in Section III and the controller introduced in Section IV are both based on a system linearized around hover conditions, the singularity-free attitude representation eases the extension to nonlinear methods in future work. A unit quaternion

$$\boldsymbol{q} = (q_0, q_1, q_2, q_3) = (\cos(\alpha/2), \boldsymbol{n}\sin(\alpha/2)) \qquad (1)$$

represents a rotation in three-dimensional space, where $\boldsymbol{n}$ is a three-dimensional unit vector denoting the rotation

[1]Throughout this paper we refer to position and attitude as the *pose*.

978-1-4673-6358-7/13/$31.00 ©2013 IEEE

axis, and α is the rotation angle [9]. (For the ease of notation, throughout this paper vectors are expressed as n-tuples $(x_1, x_2, \dots)$, with dimension and stacking clear from context.) The covariance of a quaternion that represents a small, random rotation around each axis can be modeled as

$$\boldsymbol{\Sigma}_{rot} = \begin{bmatrix} 0 & 0 & 0 & 0 \\ 0 & \sigma_q^2/4 & 0 & 0 \\ 0 & 0 & \sigma_q^2/4 & 0 \\ 0 & 0 & 0 & \sigma_q^2/4 \end{bmatrix}, \tag{2}$$

where σ_q is the standard deviation of the random rotation angle around the corresponding axis (denoted by the same variable for all axes since throughout this paper σ_q is assumed to be identical for all directions). Consequently, the covariance matrix of a rotational disturbance around an arbitrary quaternion $\boldsymbol{q}$ is given by

$$\boldsymbol{\Sigma}_q(\boldsymbol{q}) = \bar{\boldsymbol{Q}}_q(\boldsymbol{q}) \boldsymbol{\Sigma}_{rot} \bar{\boldsymbol{Q}}_q(\boldsymbol{q})^T, \tag{3}$$

where $\bar{\boldsymbol{Q}}_q(\boldsymbol{q})$ denotes the conjugate quaternion multiplication matrix [9]. For more information on unit quaternions for attitude representation, refer to [8], [9].

B. Payload Model

We consider the payload to be a dynamical structure with some characteristic deformation modes. The pose of the structure in space is described by a reference position $\boldsymbol{p}_b = (x_b, y_b, z_b)$ measured in the inertial frame I, and a reference attitude $\boldsymbol{q}_b$ defined as the rotation from the inertial frame I to the structure's body frame B. The inertial frame I is chosen such that the z-axis points upwards, i.e. gravity acts in the negative z-direction. A set of N vehicles is attached to the structure, and the pose of each vehicle is given by its position $\boldsymbol{p}_n$ and attitude $\boldsymbol{q}_n$, both expressed in the payload's body frame B. Fig. 2 shows an example of such a flying structure carried by three vehicles.

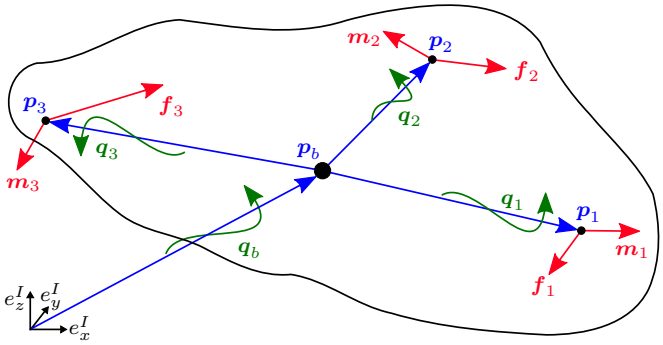

Fig. 2. Schematic illustration of the quantities that describe the model of flexible structures considered in this paper. In this example, three vehicles are attached to the payload ($N = 3$). The red arrows ($\boldsymbol{f}_n$ and $\boldsymbol{m}_n$) denote inputs and are measured in the corresponding local frame V_n of vehicle n. The blue arrows ($\boldsymbol{p}_b$ and $\boldsymbol{p}_n$) denote positions, whereat $\boldsymbol{p}_b$ is measured in the inertial frame I and $\boldsymbol{p}_n$ in the structure's body frame B. The green twisted arrows denote rotations: $\boldsymbol{q}_b$ denotes the rotation from the inertial frame I to the body frame B, and $\boldsymbol{q}_n$ are rotations from the body frame B to the vehicle frame V_n.

1) Inputs: Each vehicle produces two independent inputs: a force vector $\boldsymbol{f}_n$ and a moment vector $\boldsymbol{m}_n$, both expressed in the vehicle's local frame V_n. We define the input vector to be

$$\boldsymbol{u} = (\boldsymbol{f}_1, \dots, \boldsymbol{f}_N, \boldsymbol{m}_1, \dots, \boldsymbol{m}_N). \tag{4}$$

In order to obtain the resulting total force $\boldsymbol{f}_{tot}$ and the resulting total moment $\boldsymbol{m}_{tot}$ acting on the body's reference point, we transform each vehicle's input from the local frame V_n to the body frame B, and then sum up all components:

$$\boldsymbol{f}_{tot} = \sum_{n=1}^{N} \boldsymbol{R}(\boldsymbol{q}_n)^T \boldsymbol{f}_n, \tag{5}$$

$$\boldsymbol{m}_{tot} = \sum_{n=1}^{N} \boldsymbol{p}_n \times (\boldsymbol{R}(\boldsymbol{q}_n)^T \boldsymbol{f}_n) + \boldsymbol{R}(\boldsymbol{q}_n)^T \boldsymbol{m}_n, \tag{6}$$

where $\boldsymbol{R}(\boldsymbol{q}_n)$ denotes the orthogonal 3×3 rotation matrix for the rotation defined by $\boldsymbol{q}_n$ [9]. Equations (5) and (6) can be written in compact matrix form:

$$\begin{bmatrix} \boldsymbol{f}_{tot} \\ \boldsymbol{m}_{tot} \end{bmatrix} = \begin{bmatrix} \boldsymbol{K}_f \\ \boldsymbol{K}_m \end{bmatrix} \boldsymbol{u}, \tag{7}$$

with

$$\boldsymbol{K}_f = \begin{bmatrix} \boldsymbol{R}(\boldsymbol{q}_1)^T \cdots \boldsymbol{R}(\boldsymbol{q}_N)^T & \boldsymbol{0}_{3\times 3N} \end{bmatrix}, \tag{8}$$

$$\boldsymbol{K}_m = \begin{bmatrix} [\![\boldsymbol{p}_1 \times]\!] \boldsymbol{R}(\boldsymbol{q}_1)^T \cdots [\![\boldsymbol{p}_N \times]\!] \boldsymbol{R}(\boldsymbol{q}_N)^T, \\ \boldsymbol{R}(\boldsymbol{q}_1)^T \cdots \boldsymbol{R}(\boldsymbol{q}_N)^T \end{bmatrix}, \tag{9}$$

where $[\![\boldsymbol{p}_n \times]\!]$ denotes the cross product matrix [9]. Notice that for models where the vehicles provide fewer inputs (e.g. not a force vector, but only a force along a fixed direction), the dimension of the input map matrices $\boldsymbol{K}_f$ and $\boldsymbol{K}_m$ must be adapted, but the derivation is similar.

2) Measurements: We assume that either each vehicle provides information on its position ${}^I\boldsymbol{p}_n$ and attitude ${}^I\boldsymbol{q}_n$ with high accuracy and at a high rate, or that ${}^I\boldsymbol{p}_n$ and ${}^I\boldsymbol{q}_n$ can be measured directly. (The superscript I denotes that the quantities are expressed in the inertial frame.) The conversion of $\boldsymbol{p}_n$ and $\boldsymbol{q}_n$ to the inertial frame is given by

$${}^I\boldsymbol{p}_n = \boldsymbol{p}_b + \boldsymbol{R}(\boldsymbol{q}_b)^T \boldsymbol{p}_n, \tag{10}$$

$${}^I\boldsymbol{q}_n = \boldsymbol{q}_n \otimes \boldsymbol{q}_b, \tag{11}$$

where $\otimes$ denotes the quaternion multiplication [9].

3) System Dynamics: The translational dynamics of the payload's reference position are expressed in the inertial frame I. The acceleration is given by

$$\begin{aligned} \ddot{\boldsymbol{p}}_b &= \frac{1}{m_b} \boldsymbol{R}(\boldsymbol{q}_b)^T \boldsymbol{f}_{tot} + \boldsymbol{g} \\ &= \frac{1}{m_b} \boldsymbol{R}(\boldsymbol{q}_b)^T \boldsymbol{K}_f \boldsymbol{u} + \boldsymbol{g}, \end{aligned} \tag{12}$$

where m_b denotes the mass of the payload (including the attached vehicles), and $\boldsymbol{g} = (0, 0, -g)$ is the gravity vector. The angular dynamics are described by the current attitude $\boldsymbol{q}_b$ of the payload and its angular rates in the body frame B, denoted by $\boldsymbol{\omega}_b = (\omega_x, \omega_y, \omega_z)$. The quaternion rate is given by

$$\dot{\boldsymbol{q}}_b = \frac{1}{2} \boldsymbol{W}_q(\boldsymbol{q}_b)^T \boldsymbol{\omega}_b, \tag{13}$$

where $\boldsymbol{W}_q(\boldsymbol{q}_b)$ denotes the quaternion rate matrix [9]. If the reference position $\boldsymbol{p}_b$ does not coincide with the payload's center of gravity, a gravitational moment $\boldsymbol{m}_g$ is introduced. In the body frame B, the gravitational moment is given by

$$\boldsymbol{m}_g = \boldsymbol{p}_g \times (m_b \boldsymbol{R}(\boldsymbol{q}_b)\boldsymbol{g}), \tag{14}$$

with $\boldsymbol{p}_g = (x_g, y_g, z_g)$ being the center of gravity expressed in the body frame B. The angular acceleration is then given by Euler's equation [10]:

$$\begin{aligned}\dot{\boldsymbol{\omega}}_b &= {\boldsymbol{J}_b}^{-1}(\boldsymbol{m}_{tot} + \boldsymbol{m}_g - \boldsymbol{\omega}_b \times (\boldsymbol{J}_b \boldsymbol{\omega}_b)) \\ &= {\boldsymbol{J}_b}^{-1}(\boldsymbol{K}_m \boldsymbol{u} + \boldsymbol{p}_g \times (m_b \boldsymbol{R}(\boldsymbol{q}_b)\boldsymbol{g}) - \boldsymbol{\omega}_b \times (\boldsymbol{J}_b \boldsymbol{\omega}_b)),\end{aligned} \tag{15}$$

where $\boldsymbol{J}_b$ denotes the rotational inertia of the payload around the reference point, including the attached vehicles. $\boldsymbol{J}_b$ is assumed to be constant, i.e. the variation of $\boldsymbol{J}_b$ due to deformation of the payload is neglected.

4) Deformation Modes: In addition to the payload's body dynamics derived above, we model an arbitrary number of M deformation modes as second order systems. The deformation of each mode is parameterized by a scalar d_m, hence we can define a deformation vector

$$\boldsymbol{d} = (d_1, \ldots, d_M). \tag{16}$$

We assume that the deformation dynamics can be written in the linear form

$$\ddot{\boldsymbol{d}} = \boldsymbol{K}_e \boldsymbol{d} + \boldsymbol{K}_d \dot{\boldsymbol{d}} + \boldsymbol{K}_u \boldsymbol{u}, \tag{17}$$

where the matrices $\boldsymbol{K}_e$, $\boldsymbol{K}_d$, and $\boldsymbol{K}_u$ are characteristics of the flexible payload and of the vehicle configuration. These deformation characteristics are obtained, for example, by model-based derivations of second order deformation dynamics, or by finite element methods that numerically compute the deformation characteristics for a particular type of payload. The vehicle positions $\boldsymbol{p}_n$ and attitudes $\boldsymbol{q}_n$ may be functions of the deformation $\boldsymbol{d}$, but unless otherwise stated we assume that the deformation is small, such that $\boldsymbol{p}_n$ and $\boldsymbol{q}_n$ can be considered to be constant. Consequently, the input map matrices $\boldsymbol{K}_f$ and $\boldsymbol{K}_m$ are constant, too.

C. Linearized Payload Model

The observer and the control strategy that will be introduced in Section III and IV, respectively, are based on a linear model of the system. Therefore, we linearize the dynamics around a desired operating point.

1) Nominal State: The nominal state is chosen such that the payload hovers at some desired position without rotation relative to the inertial frame I:

$$\begin{aligned}{\boldsymbol{p}_b}^* &= (x_b^*, y_b^*, z_b^*), & \dot{\boldsymbol{p}}_b^* &= (0,0,0), \qquad (18)\\ {\boldsymbol{q}_b}^* &= (1,0,0,0), & \boldsymbol{\omega}_b{}^* &= (0,0,0). \qquad (19)\end{aligned}$$

Further, the payload is not deformed and the deformation rate is zero at the operating point:

$$\boldsymbol{d}^* = (0, \ldots, 0), \qquad \dot{\boldsymbol{d}}^* = (0, \ldots, 0). \tag{20}$$

The linearized system describes the dynamics of the state deviation $\Delta\boldsymbol{s}$ from the nominal state $\boldsymbol{s}^*$. We define the state vector as

$$\boldsymbol{s} = (\boldsymbol{p}_b, \dot{\boldsymbol{p}}_b, \tilde{\boldsymbol{q}}_b, \boldsymbol{\omega}_b, \boldsymbol{d}, \dot{\boldsymbol{d}}), \tag{21}$$

where $\tilde{\boldsymbol{q}}_b$ is the vector part of $\boldsymbol{q}_b$:

$$\tilde{\boldsymbol{q}}_b = (q_{b1}, q_{b2}, q_{b3}) = \boldsymbol{n}_b \sin(\alpha_b/2). \tag{22}$$

The reason why the state only contains the vector part of the quaternion is the following: The rotational deviation $\Delta\boldsymbol{q}_b$ is assumed to be small. By inspecting the structure of a unit quaternion (1), we see that the first element q_0 becomes constant when we linearize around zero rotation. Consequently, the first element of $\boldsymbol{q}_b$ is not a dynamic state and can be excluded from the state vector.

2) Nominal Input: At the operating point, the system should not accelerate; therefore, by solving (12), (15), and (17) to be zero and inserting the nominal state, we find that the nominal input $\boldsymbol{u}^*$ must satisfy the linear matrix equation

$$\begin{bmatrix}\boldsymbol{K}_f \\ \boldsymbol{K}_m \\ \boldsymbol{K}_u\end{bmatrix} \boldsymbol{u}^* = \begin{bmatrix}-m_b\boldsymbol{g} \\ -\boldsymbol{m}_g \\ \boldsymbol{0}_{M\times 1}\end{bmatrix}. \tag{23}$$

If (23) has no solution, then the system cannot stay at its operating point, meaning that the vehicle configuration is invalid. On the other hand, if (23) has multiple solutions, we choose, for example, the solution that minimizes the control effort $||\boldsymbol{u}^*||_2$.

3) Nominal Measurement: We define the measurement vector to be

$$\boldsymbol{y} = ({}^I\boldsymbol{p}_1, \ldots, {}^I\boldsymbol{p}_N, {}^I\boldsymbol{q}_1, \ldots, {}^I\boldsymbol{q}_N), \tag{24}$$

where ${}^I\boldsymbol{p}_n$ and ${}^I\boldsymbol{q}_n$ are given by (10) and (11). Notice that for the measurement vector all elements of the quaternions are taken into account, which has the following two reasons: Firstly, $\boldsymbol{q}_n$ is not small in general, and removing the extra constraint would be involved. Secondly, constraints in the measurement vector are not problematic; the unity constraint means only that the four elements of a measured quaternion are correlated, and this can be handled by an appropriate estimator. The nominal measurement $\boldsymbol{y}^*$ can then be computed by inserting the nominal state $\boldsymbol{s}^*$ into the measurement functions (10) and (11), which yields

$$\boldsymbol{y}^* = ({\boldsymbol{p}_b}^* + \boldsymbol{p}_1, \ldots, {\boldsymbol{p}_b}^* + \boldsymbol{p}_N, \boldsymbol{q}_1, \ldots, \boldsymbol{q}_N). \tag{25}$$

4) System Matrices: Based on the system dynamics derived above, the linear system matrix $\boldsymbol{A}$ can be obtained by differentiation of (12), (13), (15), and (17):

$$\boldsymbol{A} = \left.\frac{\mathrm{d}\dot{\boldsymbol{s}}}{\mathrm{d}\boldsymbol{s}}\right|_{\boldsymbol{s}=\boldsymbol{s}^*, \boldsymbol{u}=\boldsymbol{u}^*} = \begin{bmatrix}\boldsymbol{0} & \boldsymbol{I}_3 & \boldsymbol{0} & \boldsymbol{0} & \boldsymbol{0} & \boldsymbol{0} \\ \boldsymbol{0} & \boldsymbol{0} & \boldsymbol{A}_1 & \boldsymbol{0} & \boldsymbol{0} & \boldsymbol{0} \\ \boldsymbol{0} & \boldsymbol{0} & \boldsymbol{0} & \boldsymbol{A}_2 & \boldsymbol{0} & \boldsymbol{0} \\ \boldsymbol{0} & \boldsymbol{0} & \boldsymbol{A}_3 & \boldsymbol{0} & \boldsymbol{0} & \boldsymbol{0} \\ \boldsymbol{0} & \boldsymbol{0} & \boldsymbol{0} & \boldsymbol{0} & \boldsymbol{0} & \boldsymbol{I}_M \\ \boldsymbol{0} & \boldsymbol{0} & \boldsymbol{0} & \boldsymbol{0} & \boldsymbol{K}_e & \boldsymbol{K}_d \end{bmatrix}, \tag{26}$$

where $\boldsymbol{I}_i$ denotes an identity matrix of size i, and $\boldsymbol{0}$ denotes a zero matrix of appropriate dimension. The submatrices are given by

$$\boldsymbol{A}_1 = \frac{2}{m_b}[\![(\boldsymbol{K}_f \boldsymbol{u}^*)\times]\!]^T, \qquad \boldsymbol{A}_2 = \frac{1}{2}\boldsymbol{I}_3, \tag{27}$$

$$\boldsymbol{A}_3 = 2m_b g \boldsymbol{J}_b{}^{-1} \begin{bmatrix} z_g & 0 & 0 \\ 0 & z_g & 0 \\ -x_g & -y_g & 0 \end{bmatrix}. \tag{28}$$

We note that $\boldsymbol{A}_3$ vanishes if the reference position $\boldsymbol{p}_b$ is chosen to be the payload's center of gravity. By differentiating the dynamics with respect to the input vector, the linear input matrix $\boldsymbol{B}$ yields

$$\boldsymbol{B} = \left.\frac{\mathrm{d}\dot{\boldsymbol{s}}}{\mathrm{d}\boldsymbol{u}}\right|_{\boldsymbol{s}=\boldsymbol{s}^*,\boldsymbol{u}=\boldsymbol{u}^*} = \begin{bmatrix} \boldsymbol{0} \\ \frac{1}{m_b}\boldsymbol{K}_f \\ \boldsymbol{0} \\ \boldsymbol{J}_b{}^{-1}\boldsymbol{K}_m \\ \boldsymbol{0} \\ \boldsymbol{K}_u \end{bmatrix}. \tag{29}$$

Further, by differentiating the measurement vector (24) with respect to the state variables, we obtain the linear measurement matrix $\boldsymbol{C}$:

$$\boldsymbol{C} = \left.\frac{\mathrm{d}\boldsymbol{y}}{\mathrm{d}\boldsymbol{u}}\right|_{\boldsymbol{s}=\boldsymbol{s}^*,\boldsymbol{u}=\boldsymbol{u}^*} = \begin{bmatrix} \boldsymbol{C}_1 & \boldsymbol{0} & \boldsymbol{C}_2 & \boldsymbol{0} & \boldsymbol{C}_3 & \boldsymbol{0} \\ \boldsymbol{0} & \boldsymbol{0} & \boldsymbol{C}_4 & \boldsymbol{0} & \boldsymbol{C}_5 & \boldsymbol{0} \end{bmatrix}, \tag{30}$$

with

$$\boldsymbol{C}_1 = \begin{bmatrix} \boldsymbol{I}_3 \\ \vdots \\ \boldsymbol{I}_3 \end{bmatrix}, \quad \boldsymbol{C}_2 = \begin{bmatrix} 2[\![\boldsymbol{p}_1\times]\!]^T \\ \vdots \\ 2[\![\boldsymbol{p}_N\times]\!]^T \end{bmatrix}, \quad \boldsymbol{C}_3 = \begin{bmatrix} \mathrm{d}\boldsymbol{p}_1/\mathrm{d}\boldsymbol{d} \\ \vdots \\ \mathrm{d}\boldsymbol{p}_N/\mathrm{d}\boldsymbol{d} \end{bmatrix}, \tag{31}$$

$$\boldsymbol{C}_4 = \begin{bmatrix} \tilde{\boldsymbol{Q}}_q(\boldsymbol{q}_1) \\ \vdots \\ \tilde{\boldsymbol{Q}}_q(\boldsymbol{q}_N) \end{bmatrix}, \quad \boldsymbol{C}_5 = \begin{bmatrix} \mathrm{d}\boldsymbol{q}_1/\mathrm{d}\boldsymbol{d} \\ \vdots \\ \mathrm{d}\boldsymbol{q}_N/\mathrm{d}\boldsymbol{d} \end{bmatrix}. \tag{32}$$

$\tilde{\boldsymbol{Q}}_q(\boldsymbol{q}_n)$ denotes the quaternion multiplication matrix, with the first column omitted [9]. Notice that the matrices $\boldsymbol{C}_3$ and $\boldsymbol{C}_5$ describe the influence of the deformation $\boldsymbol{d}$ on the position $\boldsymbol{p}_n$ and attitude $\boldsymbol{q}_n$ of the vehicles. Thus, when computing $\boldsymbol{C}_3$ and $\boldsymbol{C}_5$, we do not assume $\boldsymbol{p}_n$ and $\boldsymbol{q}_n$ to be constant.

III. Estimator

In this section, we introduce a state observer that provides full state information, including the current deformation of each mode. The estimator is based upon a hybrid Kalman filter [11], meaning that the process model is continuous and the measurements arrive at discrete times. By using a hybrid Kalman filter we are not restricted to a certain constant sampling rate; measurements may arrive at irregular intervals while the covariance of the estimated state just grows continuously between incoming measurements.[2] Further, we are not constrained to discrete intervals if the estimated state is predicted into the future (e.g. for latency compensation). Since the state might not be fully observable for some vehicle configurations, we must check the system's observability before we apply the estimator.

A. Prediction

We assume that the estimator runs at a considerably higher rate than the system's natural frequencies; the predicted evolution of the estimated state deviation $\Delta\hat{\boldsymbol{s}}$ can be obtained by numerical integration of the system dynamics. Similarly, the evolution of the state covariance matrix $\boldsymbol{P}_{\hat{s}}$ is computed by integration of

$$\dot{\boldsymbol{P}}_{\hat{s}}(t) = \boldsymbol{A}\boldsymbol{P}_{\hat{s}}(t) + \boldsymbol{P}_{\hat{s}}(t)\boldsymbol{A}^T + \boldsymbol{\Sigma}_s, \tag{33}$$

where $\boldsymbol{\Sigma}_s$ is the continuous time process noise covariance matrix. The process noise is modeled as zero-mean, uncorrelated white noise processes acting on the accelerations:

$$\boldsymbol{\Sigma}_s = \mathrm{diag}(\boldsymbol{0}_{3\times3}, \sigma_{\ddot{p}}^2\boldsymbol{I}_3, \boldsymbol{0}_{3\times3}, \sigma_{\dot{\omega}}^2\boldsymbol{I}_3, \boldsymbol{0}_{M\times M}, \sigma_{\ddot{d}}^2\boldsymbol{I}_M), \tag{34}$$

where $\sigma_{\ddot{p}}$, $\sigma_{\dot{\omega}}$, and $\sigma_{\ddot{d}}$ describe the standard deviation of the noise processes for the corresponding acceleration.

B. Measurement Update

Whenever a measurement $\boldsymbol{y}_k$ arrives, we update the current estimated state and its covariance matrix. The current Kalman gain is obtained by

$$\boldsymbol{K}_{est}(t_k) = \boldsymbol{P}_{\hat{s}}(t_k)\boldsymbol{C}^T(\boldsymbol{C}\boldsymbol{P}_{\hat{s}}(t_k)\boldsymbol{C}^T + \boldsymbol{\Sigma}_y)^{-1}, \tag{35}$$

where t_k is the time at which the measurement arrives, and $\boldsymbol{\Sigma}_y$ denotes the measurement noise covariance matrix. The measurement noise covariance is modeled as

$$\boldsymbol{\Sigma}_y = \mathrm{diag}(\boldsymbol{\Sigma}_p(\boldsymbol{p}_1), \ldots, \boldsymbol{\Sigma}_p(\boldsymbol{p}_N), \boldsymbol{\Sigma}_q(\boldsymbol{q}_1), \ldots, \boldsymbol{\Sigma}_q(\boldsymbol{q}_N)), \tag{36}$$

where $\boldsymbol{\Sigma}_q(\boldsymbol{q}_n)$ is given by (3).[3] The noise on the position measurements is modeled as additive, zero-mean, uncorrelated white noise for each axis:

$$\boldsymbol{\Sigma}_p(\boldsymbol{p}_n) = \sigma_p^2\boldsymbol{I}_3, \tag{37}$$

where σ_p is the standard deviation for position measurements, being the same for all axes. The current state estimate is then updated using

$$\Delta\hat{\boldsymbol{s}}(t_{k+}) = \Delta\hat{\boldsymbol{s}}(t_{k-}) + \boldsymbol{K}_{est}(t_k)(\Delta\boldsymbol{y}_k - \boldsymbol{C}\Delta\hat{\boldsymbol{s}}(t_{k-})), \tag{38}$$

and the covariance is updated with

$$\boldsymbol{P}_{\hat{s}}(t_{k+}) = (\boldsymbol{I}_{12+2M} - \boldsymbol{K}_{est}(t_k)\boldsymbol{C})\boldsymbol{P}_{\hat{s}}(t_{k-}). \tag{39}$$

This completes the description of the observer, whose output is then fed to the controller introduced in the next section.

[2] As described in Section V, the methods presented in this paper are validated using a visual motion tracking system. Vehicles can obscure one another, resulting in occasional dropped measurements. We thus cannot assume that measurements arrive regularly.

[3] Notice that the measurement covariance matrix given by (36) is singular, since the measurement contains quaternions constrained to unity norm. However, given that the system is observable, the matrix inversion in (35) does not become singular.

IV. Controller

In this section, we describe a control strategy for guiding the flexible payload to a desired pose, while also controlling the deformation modes to zero. We assume that the controller runs at a high rate, such that it can be considered to run in continuous time. We further assume that the vehicles have been placed such that the system is controllable.

A continuous-time, infinite-horizon LQR controller is applied to control the flexible payload [12]. The LQR controller minimizes the quadratic cost

$$J = \int_{t_0}^{\infty} \Delta \boldsymbol{s}(t)^T \boldsymbol{W}_s \Delta \boldsymbol{s}(t) + \Delta \boldsymbol{u}(t)^T \boldsymbol{W}_u \Delta \boldsymbol{u}(t) \mathrm{d}t. \quad (40)$$

$\boldsymbol{W}_s$ and $\boldsymbol{W}_u$ are positive definite weight matrices that penalize state and control input deviations, respectively. The optimal state feedback gain matrix $\boldsymbol{K}_{ctr}$ is obtained by

$$\boldsymbol{K}_{ctr} = {\boldsymbol{W}_u}^{-1} \boldsymbol{B}^T \boldsymbol{X}, \quad (41)$$

where $\boldsymbol{X}$ is the positive definite solution of the continuous time algebraic Riccati equation [12]. Notice that $\boldsymbol{K}_{ctr}$ is constant and can be computed offline. The optimal control strategy is then given by the state feedback law

$$\Delta \boldsymbol{u} = -\boldsymbol{K}_{ctr} \Delta \boldsymbol{s}, \quad (42)$$

which is applied using the estimated state deviation $\Delta \hat{\boldsymbol{s}}$ delivered by the observer introduced in Section III.

V. Example: A Flying Ring

In this section, we apply the methods introduced above to a flexible ring that is carried by six quadrocopters. Fig. 1 shows a snapshot of the flying ring.

A. Vehicle Configuration

As illustrated in Fig. 3, we consider a ring with radius r. The ring's center is defined to be the reference position $\boldsymbol{p}_b$. The reference attitude $\boldsymbol{q}_b$ is chosen such that the ring lies within the body xy-plane while the body z-axis points upwards. Six vehicles are attached to the ring, distributed uniformly over its circumference. Hence, we can write

$$\boldsymbol{p}_n = (x_n, y_n, \Delta z_n(\boldsymbol{d})), \quad (43)$$

with

$$\left.\begin{aligned} \alpha_n &= (n-1)2\pi/6, \\ x_n &= r\cos(\alpha_n), \\ y_n &= r\sin(\alpha_n), \end{aligned}\right\} \text{ for } n = 1, \ldots, 6. \quad (44)$$

$\Delta z_n(\boldsymbol{d})$ denotes the displacement caused by the deformation and will be derived later. (Notice that for this example we consider only out-of-plane deformations.) To increase control authority in the horizontal plane, the vehicles are attached with a tilt angle such that their thrust contains a horizontal component. This allows the ring to accelerate horizontally without tilting. The vehicle's tilt angle β_n is chosen as

$$\beta_n = +\beta_{tilt} \quad \text{for } n = 1, 3, 5, \quad (45)$$

$$\beta_n = -\beta_{tilt} \quad \text{for } n = 2, 4, 6. \quad (46)$$

The value of the tilt angle β_{tilt} is a design parameter; for the experiments presented herein we chose $\beta_{tilt} = \pi/4$. The attitude of vehicle n relative to the ring can be written as

$$\boldsymbol{q}_n = \boldsymbol{q}_y(\beta_n) \otimes \boldsymbol{q}_z(\alpha_n) \otimes \Delta \boldsymbol{q}_n(\boldsymbol{d}), \quad (47)$$

where $\boldsymbol{q}_y$ and $\boldsymbol{q}_z$ denote rotations around the current y and z-axis, respectively, and $\Delta \boldsymbol{q}_n(\boldsymbol{d})$ denotes the rotation caused by the deformation relative to the body frame B.

B. Inputs

For this example, we define that each vehicle provides two scalar inputs: the thrust force $f_{z,n}$ along its z-axis, and a roll moment $m_{x,n}$ around its x-axis. This is motivated by the fact that fixed-rotor quadrocopters can generate thrust force only along their z-axis. Further, they can only provide small moments around their z-axis. Therefore, the yaw of the ring is controlled by the roll moments $m_{x,n}$ of the vehicles (which is possible because the vehicles are tilted). The input vector yields

$$\boldsymbol{u} = (f_{z,1}, \ldots, f_{z,6}, m_{x,1}, \ldots, m_{x,6}). \quad (48)$$

C. Deformation Modes of the Ring

Previous flights and considerations of first-principle ring dynamics suggest that the second out-of-plane mode is the critical one.[4] The deflection of the vehicles caused by the second out-of-plane mode can be written as

$$\Delta z_n(\boldsymbol{d}) = d_1 \cos(2\alpha_n) + d_2 \sin(2\alpha_n), \quad (49)$$

where α_n is given by (44) and $\boldsymbol{d} = (d_1, d_2)$ is the deformation vector. The derivative of the deformation offset with respect to the deformation parameters yields

$$\left.\frac{\mathrm{d}\boldsymbol{p}_n}{\mathrm{d}\boldsymbol{d}}\right|_{\boldsymbol{d}=\boldsymbol{0}} = \begin{bmatrix} 0 & 0 \\ 0 & 0 \\ \cos(2\alpha_n) & \sin(2\alpha_n) \end{bmatrix}. \quad (50)$$

[4]Notice that, for a thin ring, the zeroth out-of-plane mode is a translation along the z-axis and the first out-of-plane mode is a tilt rotation, both being rigid body operations.

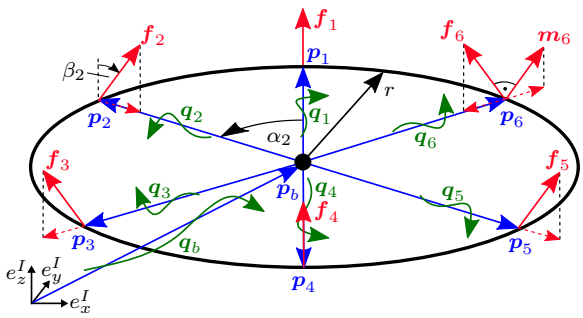

Fig. 3. Schematic illustration of the flying ring with six attached quadrocopters. The blue arrows ($\boldsymbol{p}_b$ and $\boldsymbol{p}_n$) denote positions, and the green twisted arrows ($\boldsymbol{q}_b$ and $\boldsymbol{q}_n$) are rotations. Each vehicle produces a thrust force $\boldsymbol{f}_n$ along its local z-axis, and a moment $\boldsymbol{m}_n$ along its local x-axis, denoted by the red arrows. For reasons of readability, the angles α_n and β_n are drawn only for vehicle $n = 2$, and the input moment $\boldsymbol{m}_n$ is drawn only for vehicle $n = 6$.

An excited deformation varies also the attitude of the vehicles; they are tilted around the ring's x and y-axis. We denote these two deviation angles as γ_x and γ_y. For a given point on the ring, γ_x and γ_y can be computed by constructing the plane that contains both the line tangent to the ring at that particular point, and the ring's center point. The tilt angle of the resulting plane around the x and y-axis represents the deviation angles γ_x and γ_y, respectively. The computation of these angles is involved, therefore a mathematical toolbox for symbolic computation is used [13]. The results are that γ_x and γ_y are given by

$$\begin{aligned}\tan(\gamma_x) = &(2d_2x_n + d_1y_n)\cos(2\alpha_n)/r^2 \\ &- (2d_1x_n - d_2y_n)\sin(2\alpha_n)/r^2, \qquad (51)\\ \tan(\gamma_y) = &-(d_1x_n - 2d_2y_n)\cos(2\alpha_n)/r^2 \\ &- (d_2x_n + 2d_1y_n)\sin(2\alpha_n)/r^2. \qquad (52)\end{aligned}$$

Since γ_x and γ_y are assumed to be small, the rotation caused by the deformation can be written as two subsequent rotations around the corresponding axis:

$$\Delta\boldsymbol{q}_n(\boldsymbol{d}) = \boldsymbol{q}_x(\gamma_x) \otimes \boldsymbol{q}_y(\gamma_y). \qquad (53)$$

Consequently, taking the derivative of (47) with respect to $\boldsymbol{d}$ at the operating point $\boldsymbol{d} = \boldsymbol{0}$ yields

$$\left.\frac{\mathrm{d}\boldsymbol{q}_n}{\mathrm{d}\boldsymbol{d}}\right|_{\boldsymbol{d}=\boldsymbol{0}} = \boldsymbol{q}_y(\beta_n) \otimes \boldsymbol{q}_z(\alpha_n) \otimes \begin{bmatrix} 0 & 0 \\ \frac{y_n\cos(2\alpha_n) - 2x_n\sin(2\alpha_n)}{2r^2} & \frac{2x_n\cos(2\alpha_n) + y_n\sin(2\alpha_n)}{2r^2} \\ \frac{x_n\cos(2\alpha_n) + 2y_n\sin(2\alpha_n)}{-2r^2} & \frac{2y_n\cos(2\alpha_n) - x_n\sin(2\alpha_n)}{2r^2} \\ 0 & 0 \end{bmatrix}, \qquad (54)$$

where a quaternion multiplication is executed for each column of the 4×2 matrix at the end of the equation.

We model the bending mode dynamics as decoupled from each other, and we assume that they are subject to linear elasticity and linear damping:

$$\ddot{\boldsymbol{d}} = \underbrace{\begin{bmatrix} k_e & 0 \\ 0 & k_e \end{bmatrix}}_{\boldsymbol{K}_e} \boldsymbol{d} + \underbrace{\begin{bmatrix} k_d & 0 \\ 0 & k_d \end{bmatrix}}_{\boldsymbol{K}_d} \dot{\boldsymbol{d}} + \boldsymbol{K}_u\boldsymbol{u}. \qquad (55)$$

A mode is excited if a vehicle produces thrust along the direction of the corresponding deviation. Therefore, based on (49), the input mapping matrix $\boldsymbol{K}_u$ is modeled as

$$\boldsymbol{K}_u = k_u\cos(\beta_{tilt}) \begin{bmatrix} \cos(2\alpha_1) \cdots \cos(2\alpha_6) & \boldsymbol{0}_{1\times 6} \\ \sin(2\alpha_1) \cdots \sin(2\alpha_6) & \boldsymbol{0}_{1\times 6} \end{bmatrix}, \qquad (56)$$

where the constant factor k_u is a characteristic of the ring. It is assumed that the input moments $m_{x,n}$ do not excite the deformation modes.

D. Parameter Values

An aluminum ring with radius $r = 1\,\mathrm{m}$ and mass $m_r = 0.54\,\mathrm{kg}$ is used for the experiments. Each of the attached vehicles weighs $m_v = 0.47\,\mathrm{kg}$. This yields the payload inertia properties

$$J_{xx} = 1.68\,\mathrm{kg\,m^2}, \qquad J_{yy} = 1.68\,\mathrm{kg\,m^2}, \qquad (57)$$
$$J_{zz} = 3.36\,\mathrm{kg\,m^2}, \qquad m_b = 3.36\,\mathrm{kg}, \qquad (58)$$

where standard moment of inertia formulas have been applied [14], and the vehicles are modeled as point masses. Based on first-principle ring dynamics [15] and measurement data analysis, the deformation parameters are estimated as

$$k_e = -0.8\,\mathrm{s^{-2}}, \;\; k_d = -0.3\,\mathrm{s^{-1}}, \;\; k_u = 0.2\,\mathrm{kg^{-1}}. \qquad (59)$$

The process noise standard deviations used in the estimator are

$$\sigma_{\ddot{p}} = 0.1\,\mathrm{m\,s^{-2}}, \;\; \sigma_{\dot{\omega}} = 0.1\,\mathrm{s^{-2}}, \;\; \sigma_{\ddot{d}} = 1\,\mathrm{m\,s^{-2}}, \qquad (60)$$

where a large value for $\sigma_{\ddot{d}}$ is chosen to account for the high uncertainty in the deformation parameters (59). The measurements have the standard deviations

$$\sigma_p = 0.02\,\mathrm{m}, \;\; \sigma_q = 0.03\,\mathrm{rad}. \qquad (61)$$

The weight matrix $\boldsymbol{W}_s$ of the LQR controller is chosen to be an identity matrix (with the corresponding SI-units), except for position deviations that are penalized more:

$$w_p = 100\,\mathrm{m^{-2}s^{-1}}. \qquad (62)$$

The input weight matrix $\boldsymbol{W}_u$ is also diagonal with

$$w_f = 1\,\mathrm{N^{-2}s^{-1}}, \;\; w_m = 15\,\mathrm{N^{-2}m^{-2}s^{-1}}, \qquad (63)$$

where w_f denotes the weight on the thrust inputs, and w_m the weight on the moment inputs. Since w_m is chosen to be high in order to avoid motor saturation, the ring's yaw errors are compensated slowly.

E. Experimental Setup

The experiments are carried out in the Flying Machine Arena at ETH Zurich [16]. We use modified Ascending Technologies 'Hummingbird' quadrocopters [17] with custom electronics. A low-latency radio link sends control commands to the vehicles at a rate of $50\,\mathrm{Hz}$. Each vehicle's absolute position and attitude is measured by an overhead infrared motion-tracking system at a rate of up to $200\,\mathrm{Hz}$.

F. Experimental Results

Fig. 4 shows the trajectories for a step in desired position, whereat the methods introduced in this paper are applied; the deformations are observed and controlled to zero. The ring tilts in order to accelerate towards the desired direction of the step, and the imbalance of thrust excites the deformation modes. However, since the deformations are observed, the controller (in combination with the elastic forces) is able to control them back to zero.

For comparison, Fig. 5 illustrates position and deformation trajectories resulting from an experiment involving a rigid body controller. The control strategy described in Section IV is applied but no deformation is modeled ($M = 0$). This is equivalent to an LQR controller for a rigid body in three-dimensional space. The same ring is used as in Fig. 4 and the

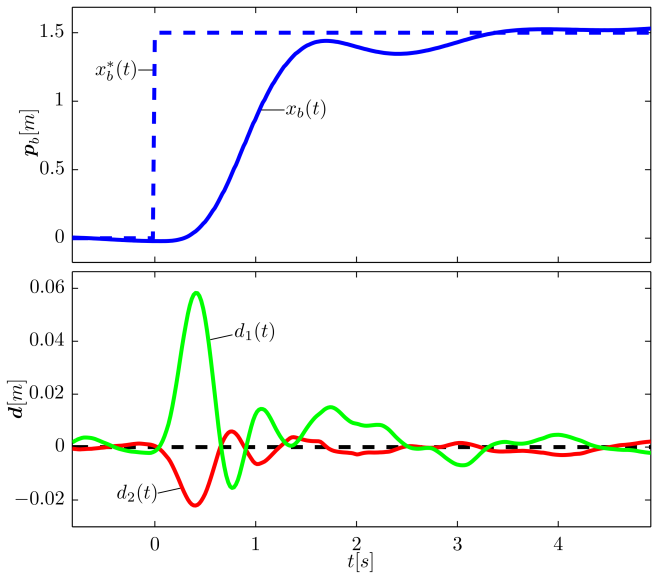

Fig. 4. Response of a flexible flying ring carried by six rigidly attached quadrocopters for a step of 1.5 m in desired x-position. In the upper plot, the dashed line represents the target x-position, and the solid line denotes the actual (estimated) position of the ring. In the lower plot, the deformation trajectories are drawn. The ring is bent while it tilts, but the deformation is controlled back to zero after some seconds. Notice that the scale of the axes is not the same as in Fig. 5.

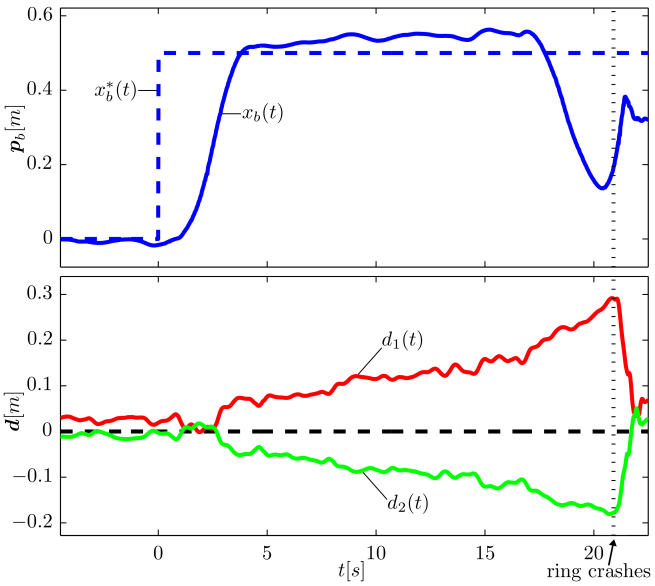

Fig. 5. Step response of the flying ring for a step of 0.5 m in x-position. An LQR controller based on the rigid body assumption is applied. The dashed line in the upper plot denotes the target x-trajectory, and the solid line shows the actual (estimated) x-trajectory. The lower plot illustrates the trajectories of the deformation parameters. After the step, the deformations grow as they are not controlled to zero, and eventually cause the ring to crash. Notice that the scale of the axes is not the same as in Fig. 4.

controller's weight matrices $\boldsymbol{W}_s$ and $\boldsymbol{W}_u$ are also identical, except that $\boldsymbol{W}_s$ is of smaller dimension since it has no entries for the deformations. Fig. 5 shows that, even after a small step in desired position, the deformations become unstable and the ring eventually crashes.

VI. Conclusion and Outlook

We have introduced a method for carrying a flexible payload using multiple flying vehicles. The method is based on common techniques and has been validated by carrying a flexible ring, a task where controllers that rely on the rigid body assumption fail. Future work to extend and improve the method includes: The linear system matrices of the flying payload derived in Section II are sparse, therefore the structural controllability theorem [18] might be applied to investigate for which conditions a particular vehicle configuration provides a structural controllable system. Furthermore, in this paper we assumed the configuration of how the vehicles are attached to the payload to be given; a future subject of study will be the development of a strategy to optimize the configuration for a particular task, while guaranteeing observability and controllability of the system. Finally, for some applications (e.g. if the payload must be deposited with a particular attitude) the presented linear methods may not be suitable, hence a nonlinear extension of this work is required.

References

[1] N. Michael, J. Fink, and V. Kumar, "Cooperative manipulation and transportation with aerial robots," *Autonomous Robots*, vol. 30, 2011.

[2] M. Bernard and K. Kondak, "Generic slung load transportation system using small size helicopters," in *Robotics and Automation, 2009. ICRA '09. IEEE International Conference on*, 2009.

[3] D. Mellinger, M. Shomin, N. Michael, and V. Kumar, "Cooperative grasping and transport using multiple quadrotors," in *Distributed Autonomous Robotic Systems*, ser. Springer Tracts in Advanced Robotics. Springer Berlin Heidelberg, 2013, vol. 83.

[4] V. Parra-Vega, A. Sanchez, C. Izaguirre, O. Garcia, and F. Ruiz-Sanchez, "Toward aerial grasping and manipulation with multiple UAVs," *Journal of Intelligent & Robotic Systems*, vol. 70, 2013.

[5] F. Gramazio, M. Kohler, and R. D'Andrea, *Flight Assembled Architecture*. Editions Hyx, Orléans, 2013.

[6] D. Sun, J. Mills, and Y. Liu, "Position control of multiple robots manipulating a flexible payload," in *American Control Conference, 1998. Proceedings of the 1998*, vol. 1, 1998.

[7] D. Economou, C. Lee, C. Mavroidis, and I. Antoniadis, "Robust vibration suppression in flexible payloads carried by robot manipulators using digital filtering of joint trajectories," in *Proceedings of the 2000 International Symposium on Robotics and Automation*, 2000.

[8] J. Stuelpnagel, "On the parametrization of the three-dimensional rotation group," *SIAM review*, vol. 6, no. 4, 1964.

[9] J. Diebel, "Representing attitude: Euler angles, unit quaternions, and rotation vectors," *Matrix*, 2006.

[10] P. H. Zipfel, *Modeling and Simulation of Aerospace Vehicle Dynamics (Aiaa Education)*. American Institute of Aeronautics & Astronautics, 2003.

[11] T. Kailath, A. H. Sayed, and B. Hassibi, *Linear Estimation*. Prentice Hall Information and System Science Series, 1999.

[12] H. P. Geering, *Optimal Control with Engineering Applications*. Springer, 2007.

[13] Wolfram Research, "Mathematica, Version 8.0," 2010.

[14] S. Bhavikatti, *A Textbook Of Engineering Mechanics (As Per Jntu Syllabus)*. New Age International (P) Limited, 2007.

[15] A. Nayfeh and P. Pai, *Linear and Nonlinear Structural Mechanics*, ser. Wiley Series in Nonlinear Science. Wiley, 2008.

[16] S. Lupashin and R. D'Andrea, "Adaptive fast open-loop maneuvers for quadrocopters," *Autonomous Robots*, vol. 33, 2012.

[17] D. Gurdan, J. Stumpf, M. Achtelik, K.-M. Doth, G. Hirzinger, and D. Rus, "Energy-efficient autonomous four-rotor flying robot controlled at 1 khz," in *IEEE International Conference on Robotics and Automation*, 2007.

[18] C.-T. Lin, "Structural controllability," *Automatic Control, IEEE Transactions on*, vol. 19, no. 3, 1974.